An empirical study of ISAC channel characteristics with human target impact at 105 GHz

Wenjun Chen[1], Yuxiang Zhang[1], Yameng Liu[1], Jianhua Zhang[1], Huiwen Gong[1], Tao Jiang[2], and Liang Xia[2]

[1]Beijing University of Posts and Telecommunications
[2]China Mobile Research Institute

July 16, 2024

Abstract

Leveraging the ultra-wideband advantages of the Terahertz (THz) band, Integrated Sensing and Communication (ISAC) facilitates high-precision sensing demands in human smart home applications. ISAC channel characteristics are the basis for ISAC system design. Currently, the ISAC channel is divided into target and background channels. Existing researches primarily focus on the attributes of human target itself, e.g., radar cross-section and Micro-Doppler effect. However, the impact of human target on neither the pathloss characteristic of background channel nor the multipath propagation characteristic of target channel is considered. To address the gap, we conduct indoor channel measurements at 105 GHz to investigate the ISAC channel characteristics with the impact of human target. Firstly, by analyzing the power angular delay profiles with and without human target, we observe the changes in quantity and power of multipath components (MPCs). Then, we propose a parameter called power control factor (PCF) to evaluate the human target impact on pathloss, thereby modifying the existing pathloss model of background channel. Eventually, we extract the MPCs belonging to target channel within target-oriented power delay profile to count the power proportion of each bounce MPCs of the target-Rx link, which supports the necessity of multi-bounce (indirect) paths modeling in target channel.

Hosted file

`el-author.cls` available at https://authorea.com/users/804587/articles/1192090-an-empirical-study-of-isac-channel-characteristics-with-human-target-impact-at-105-ghz

Hosted file

`sample.tex` available at https://authorea.com/users/804587/articles/1192090-an-empirical-study-of-isac-channel-characteristics-with-human-target-impact-at-105-ghz

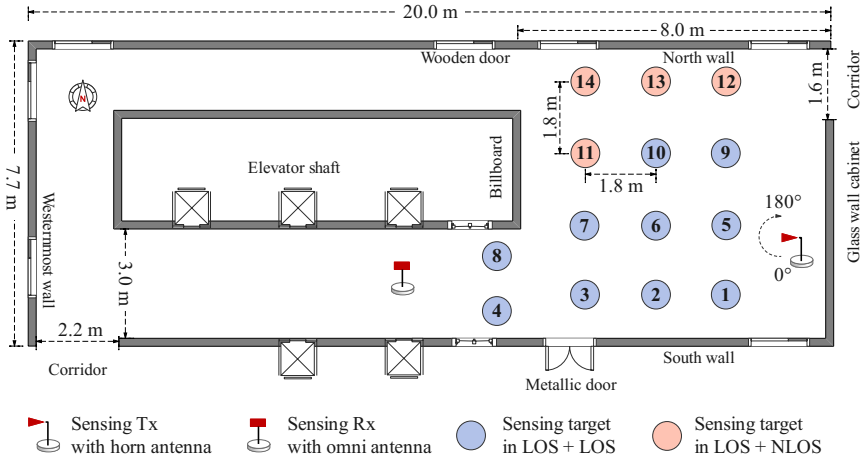

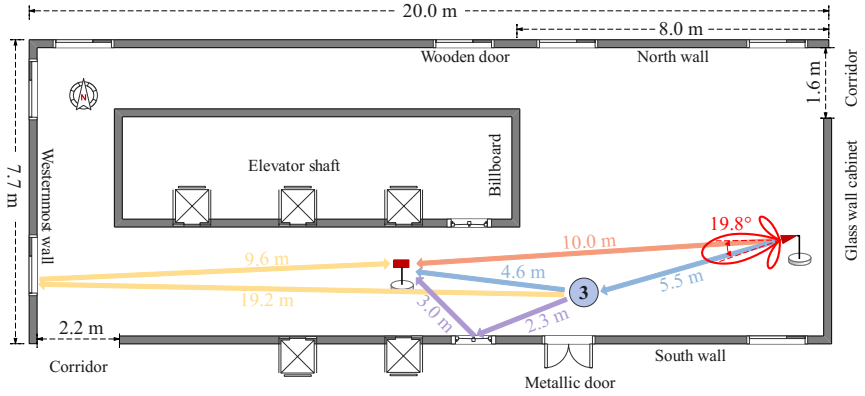

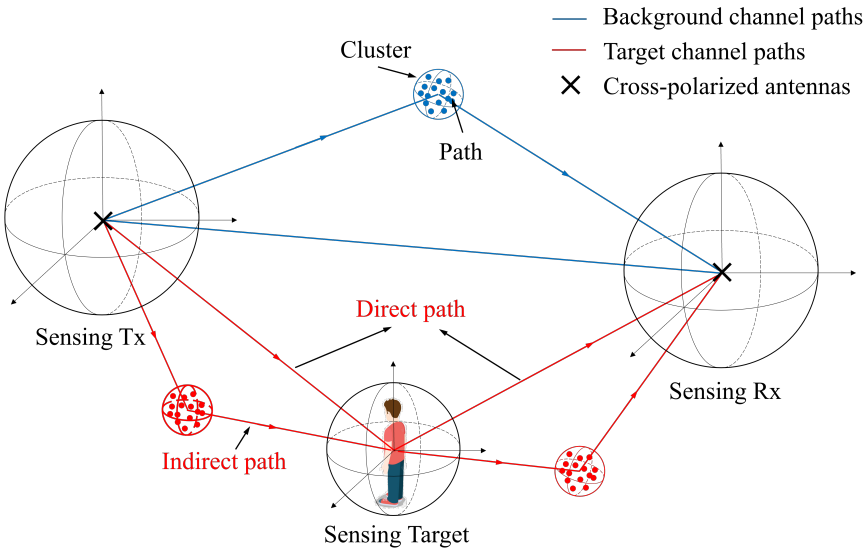

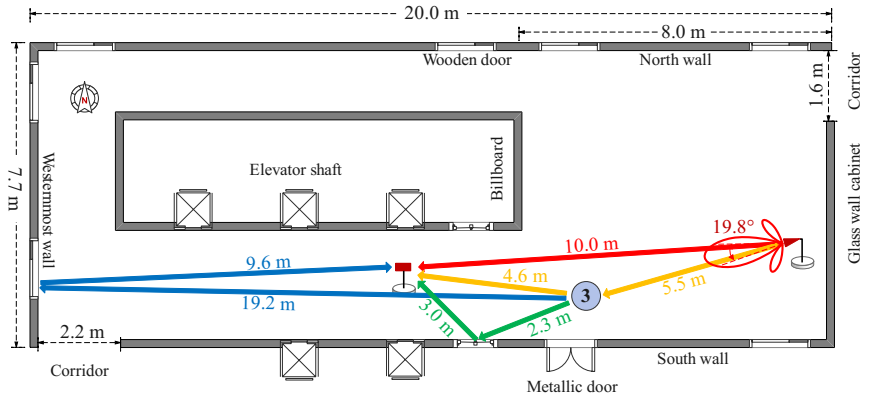

figures/MPCs3/MPCs3-eps-converted-to.pdf

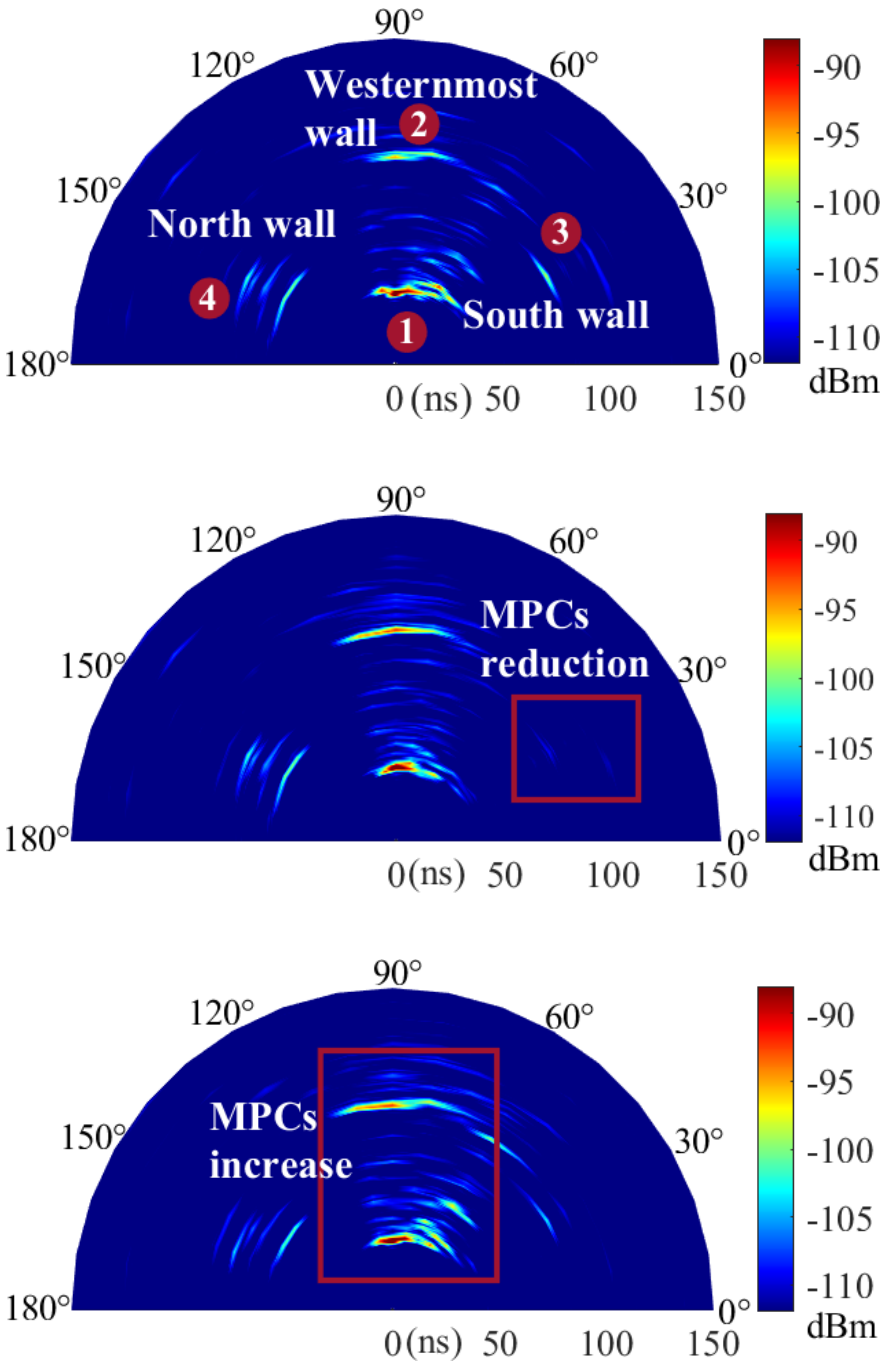

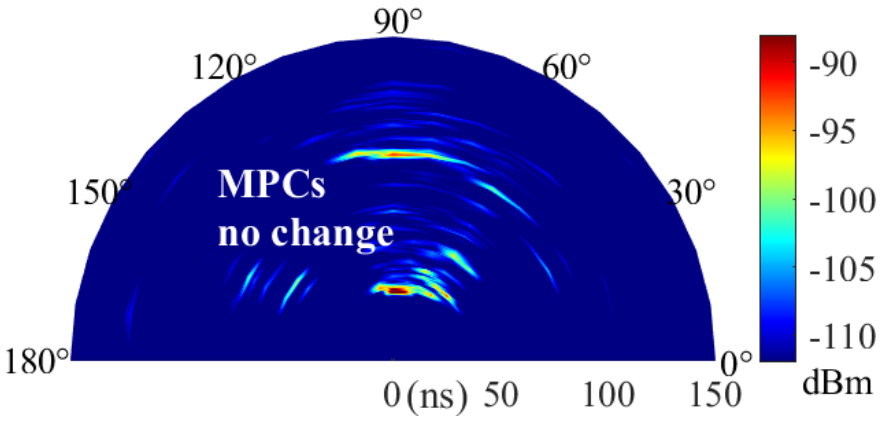

figures/factor/factor-eps-converted-to.pdf

An empirical study of ISAC channel characteristics with human target impact at 105 GHz

Wenjun Chen, Yuxiang Zhang, Yameng Liu, Jianhua Zhang✉, Huiwen Gong, Tao Jiang and Liang Xia

Leveraging the ultra-wideband advantages of the Terahertz (THz) band, Integrated Sensing and Communication (ISAC) facilitates high-precision sensing demands in human smart home applications. ISAC channel characteristics are the basis for ISAC system design. Currently, the ISAC channel is divided into target and background channels. Existing researches primarily focus on the attributes of human target itself, e.g., radar cross-section and Micro-Doppler effect. However, the impact of human target on neither the pathloss characteristic of background channel nor the multipath propagation characteristic of target channel is considered. To address the gap, we conduct indoor channel measurements at 105 GHz to investigate the ISAC channel characteristics with the impact of human target. Firstly, by analyzing the power angular delay profiles with and without human target, we observe the changes in quantity and power of multipath components (MPCs). Then, we propose a parameter called power control factor (PCF) to evaluate the human target impact on pathloss, thereby modifying the existing pathloss model of background channel. Eventually, we extract the MPCs belonging to target channel within target-oriented power delay profile to count the power proportion of each bounce MPCs of the target-Rx link, which supports the necessity of multi-bounce (indirect) paths modeling in target channel.

Introduction: Smart home is an attractive vision of future 6G network, providing intelligent services to humans such as intruder detection and health detection [1, 2]. The Integrated Sensing and Communication (ISAC) technology with Terahertz band (0.1-10 THz) is poised to meet the sensing demands of centimeter-precision and millisecond-latency, which has a superior prospect in indoor scenario [3].

The characteristics and models of ISAC channel determine the design, deployment, and performance of ISAC system [4]. The sensing ability and integration bring new characteristics to the ISAC channel, including the Radar Cross Section (RCS) of sensing target and background effect, which have not been portrayed by the traditional communication channel [5]. Further, the ISAC channel is divided into a target-related target channel and a target-independent background channel. Besides, in the radar sensing domain, the focus is on extracting target information embedded in the echo signal, such as distance, radial velocity, and RCS. Although there are some empirical models, they are applicable only when viewing the ground or sea from high altitudes [6]. However, the indoor scenario is small in scale and full of Environmental Objects (EOs), leading to an inevitable coupling of human targets and background. Therefore, the impact of human target on the indoor ISAC channel characteristics remains some gaps, necessitating more in-depth study.

Many ISAC channel measurements with human targets have been conducted in recent years. The authors in [7] measure the scattering pattern of electromagnetic signals by human body from various angles at 140 and 220 GHz. In [8], high-precision and muti-angle imaging of a walking human is realized by THz radar at 330 GHz band. [9] detects and investigates the time-varying features in dynamic channel due to human activities. Those empirical works focus on the properties of the human target itself, e.g., the RCS and Micro Doppler features. They neglect to incorporate the human target as a vital component within realistic ISAC channel. Furthermore, there is also a proliferation of studies on ISAC channel characteristics and modeling. For instance, [10] assumes the sensing signal model as two separate parts, the Line-of-Sight (LOS) link as the target channel and the Non-Line-of-Sight (NLOS) link as the clutter. In [11], the ISAC channel is modeled as a superposition of the channel coefficients of each target and the background and applies the communication channel as the latter. The author of [12] proposes an ISAC channel model which is the direct combination of the target channel and the background channel, with the latter reusing the 3GPP TR 38.901 model. However, those proposed models characterize the ISAC channel as an independent superposition of target channel and background channel. The coupling between these two channels has not been explored in the indoor scenario. Therefore, it is necessary to study the impact of human targets on the indoor ISAC channel characteristics.

Hence, this letter aims to fill the aforementioned gaps through an ISAC channel measurement campaign at 105 GHz. Through the comparative analysis of power angular delay profile (PADP) with and without human target, the changes in quantity and power of MPCs are observed. Then, a new parameter called power control factor (PCF) is proposed to evaluate the impact of human target on channel pathloss, and modify the pathloss model of background channel. Further, the propagation paths are traced within the measurement scenario with human target and confirmed by the target-oriented power delay profiles (PDP). Finally, the power proportion of each bounce MPCs of target-receiver (Rx) link is quantified, thereby supporting the multi-bounce (indirect) paths modeling in target channel.

Channel measurements campaign: The ISAC channel measurement is carried out at 105 GHz in an indoor hall, as shown in Fig. 1(a). An adult male with a height of 1.7 m and a shoulder width of 0.4 m is chosen as the sensing target. The campaign is conducted through the THz channel measurement platform, which is based on the principle of time-domain spread spectrum sliding correlation. The main equipment consists of a vector signal generator and a spectrum analyzer. Detailed parameters of measurement configuration are listed in Table 1.

Table 1: Measurement configuration

Parameters	Value/Type
Center frequency	105 GHz
Bandwidth	1.2 GHz
IF / OF frequency	12 / 31 GHz
Symbol rate	600 Msym/s
PN sequence length	511
Tx / Rx antenna type	Horn / Omni
Tx Azim. HPBW	9.9°
Antenna height	1.4 m
Polarization	Vertical

The measurement layout is illustrated in Fig. 1(b). The locations of sensing transmitter (Tx) and Rx are labeled on the diagram and are 10 m apart. These round dots with serial numbers represent different positions of the human target. According to the conditions of Tx-Target and Target-Rx links, the positions of the human target are divided into LOS+LOS and LOS+NLOS conditions. In the measurement, the human target is positioned at different measurement positions while remaining stationary and facing east. The Tx rotates horizontally the horn antenna clockwise from 0° to 180° in steps of 10°. Besides, a controlled measurement is repeated in a consistent environment without the human target.

(a)

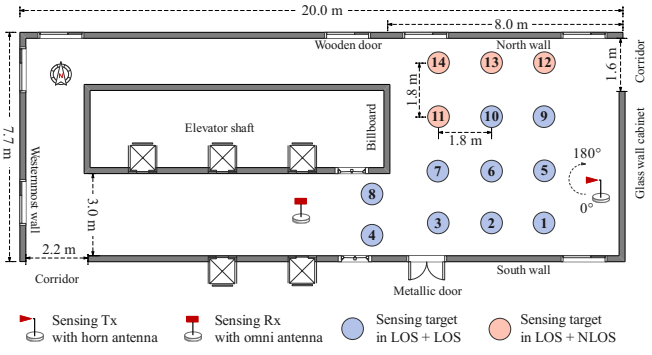

(b)

Fig. 1: Illustration of the ISAC channel measurement campaign, (a) the measurement scenario at position 6, (b) the measurement scheme.

ISAC channel characterization and modeling: This letter considers a transceiver-separated bi-static ISAC channel model, and the sensing Tx and Rx are equipped with single antennas. Up to now, it is widely accepted that the ISAC channel is composed of two components, the target channel and the background channel [11, 12]. The target channel includes all MPCs impacted by the sensing targets, while the background channel includes other MPCs not belonging to target channel within the ISAC channel. Thus, the channel impulse response (CIR) of ISAC channel can be expressed as

$$\begin{aligned}\mathbf{H}_{\mathrm{ISAC}}(\tau,t) &= PL_{\mathrm{isac}}\mathbf{H}_{\mathrm{isac}}(\tau,t) \\ &= \underbrace{\sum_{i=1}^{N} PL_{\mathrm{tar}}^{i}\mathbf{H}_{\mathrm{tar}}^{i}(\tau,t)}_{\text{Target Channel}} + \underbrace{PL_{\mathrm{bg}}\mathbf{H}_{\mathrm{bg}}(\tau,t)}_{\text{Background Channel}},\end{aligned} \tag{1}$$

where the specific meanings of the symbols are as follows,

- $\mathbf{H}_{\mathrm{ISAC}}(\tau,t)$ is the CIR of ISAC channel, and τ is the path delay.
- PL_{isac} and $\mathbf{H}_{\mathrm{isac}}(\tau,t)$ represent the pathloss and coefficient of the ISAC channel, respectively.
- i is the index of sensing target and the maximum is N.
- PL_{tar}^{i} and $\mathbf{H}_{\mathrm{tar}}^{i}(\tau,t)$ are the pathloss and coefficient of the i-th link of target channel, regardless of the correlation between different links.
- PL_{bg} and $\mathbf{H}_{\mathrm{bg}}(\tau,t)$ represent the pathloss and coefficient of the background channel, respectively.

For a single-target scenario, e.g., a human indoors, the ISAC channel model is illustrated with Fig. 2. In target channel, the Tx→human target→Rx path is defined as the direct path, while the other paths are called the indirect paths. Based on the channel measurements, the ISAC channel characteristics with human target impact, i.e., pathloss characteristic of background channel and indirect paths characteristic of target channel are investigated.

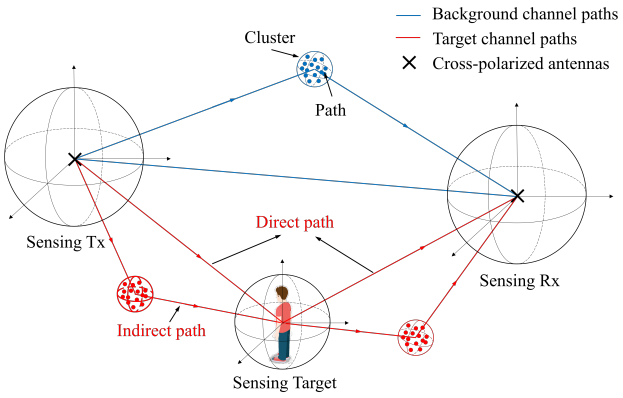

Fig. 2: Illustration of the ISAC channel model, where the blue lines denote the MPCs in background channel, and the red lines denote the MPCs in target channel.

Pathloss characteristic of background channel: To visualize the distribution of MPCs across delay, spatial, and power domains, Fig. 3 presents the PADPs under various conditions [13]. Fig. 3(a) shows the PADP of environment channel, which will be referred to later as the initial background channel. As shown in Fig. 3(a), the path with the strongest power in the center is the LOS path between Tx and Rx. In addition, labels 1 and 2 consist of single-bounce paths interacting with the south wall and the westernmost wall, respectively. The MPCs around label 3 result from multiple-bounce paths forth and back between the south wall and the north wall, owing to their high delays and low powers. Label 4 represents multiple-bounce paths, with the first bounce occurring via the north wall. This is because the horn antenna is oriented towards the north wall at this angle, making it invisible to the Rx. These observations imply that the THz ISAC channel accurately captures the major EOs.

Without loss of generality, the PADPs of sensing target in position 1, 6 and 13 are shown in Fig. 3(b)-3(d). In Fig. 3(b), the MPCs in the red square box area are significantly reduced compared to Fig. 3(a). This is mainly because the presence of sensing target attenuates the previous target-oriented signals from Tx to south wall and obscures the signals originally scattered from south wall. In Fig. 3(c), on the contrary, it appears that the MPCs in the marked area have increased relatively due to the contribution of human target. In Fig. 3(d), however, no difference is observed by comparing with Fig. 3(a), since the human target is in LOS+NLOS condition and far away from the transceiver, leading to a very low impact. When the sensing target is introduced or its position changes, the target-related MPCs will vary (corresponding to the marked area in Fig. 3), and the environment-related MPCs will change accordingly. In a word, any alteration in the target channel may invariably result in a corresponding change of the background channel. The relationship between the sensing target and the background environment is still a complex issue. Therefore, it may not be precise enough to model the ISAC channel as a simple independent superposition of target response and environmental response.

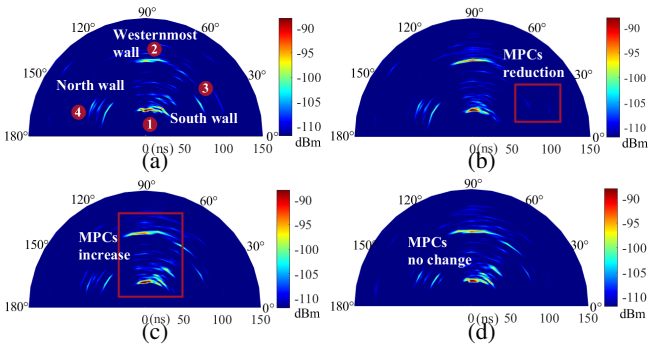

Fig. 3: Illustration of PADPs under various channel conditions. (a) the original background environment, while (b) the sensing target at measurement position 1, (c) position 6, and (d) position 13.

On the basis of above observations, the introduction of human target leads to changes in the quantity and power of MPCs, which ultimately manifest as an alteration in the channel pathloss. Based on the physical reality, a large-scale parameter called PCF is proposed to characterize the power impact of one human target (i.e., $N=1$ in (1)) on the initial background channel, which is defined as

$$O_{\mathrm{isac}} = \frac{PL_{\mathrm{isac}} - PL_{\mathrm{tar}}}{PL_{\mathrm{bg}}^{38.901}}, \tag{2}$$

where the O_{isac} denotes the PCF, the PL_{isac} and PL_{tar} represent the pathloss of the ISAC channel and target channel, respectively. The $PL_{\mathrm{bg}}^{38.901}$ is the pathloss of initial background channel, implying it is reused the pathloss model in 3GPP TR 38.901 [14].

Obviously, PL_{isac} and $PL_{\mathrm{bg}}^{38.901}$ correspond to the channel pathloss obtained from measurement with and without human target, respectively. However, as target channel is a part of the ISAC channel, it is slightly cumbersome to distinguish the MPCs subordination of target channel and background channel through measurement data processing. To get the PCF values in this measurement, one key problem to be solved is the separation of the target channel from the overall ISAC channel. Since human target is univariate, so it is reasonable to classify the relatively changed MPCs as belonging to target channel. According to this logic, the effective MPCs are needed to be extracted from the PADPs first. A synthesis procedure proposed in [15] can eliminate the interfering MPCs caused by rotational measurements. Then, the pre-processed MPCs are compared based on the absolute delay, angle of departure (AOD), and power information, and those belonging to target channel are picked out for the calculation of pathloss. By processing the measurement data in this way, the O_{isac} under 14 positions are calculated by (2) and summarised in Table 2.

Observing the table 2, there is an interesting phenomenon. The O_{isac} values are usually below 0.9 and even down to 0.6 when the human target is in LOS+LOS condition, but almost all above 0.9 when in LOS+NLOS condition. So, it is reasonable to classify them according to the condition of human target. The cumulative distribution function (CDF) of the O_{isac} values is displayed in Fig. 4. The O_{isac} values in two conditions have a significant dividing line in numerical distribution. Further, the normal distribution model is used to fit well with them, and the fitted results are shown as the dashed lines in Fig. 4. In this measurement, the O_{isac} in LOS+LOS condition obey the normal distribution $O_{\mathrm{isac}} \sim \mathcal{N}(0.817, 0.085^2)$, while in LOS+NLOS condition it obeys the normal distribution $O_{\mathrm{isac}} \sim \mathcal{N}(0.915, 0.026^2)$. That is to say, the human target in LOS+NLOS condition has less impact on the initial channel than in

LOS+LOS condition, which means the former is less easily sensed by the sensing Rx.

Table 2: The value of PCF at each measurement position

Position	Condition	O_{isac}	Position	Condition	O_{isac}
1	LOS+LOS	0.89	8	LOS+LOS	0.78
2	LOS+LOS	0.73	9	LOS+LOS	0.91
3	LOS+LOS	0.67	10	LOS+LOS	0.93
4	LOS+LOS	0.75	11	LOS+NLOS	0.89
5	LOS+LOS	0.84	12	LOS+NLOS	0.90
6	LOS+LOS	0.81	13	LOS+NLOS	0.92
7	LOS+LOS	0.86	14	LOS+NLOS	0.95

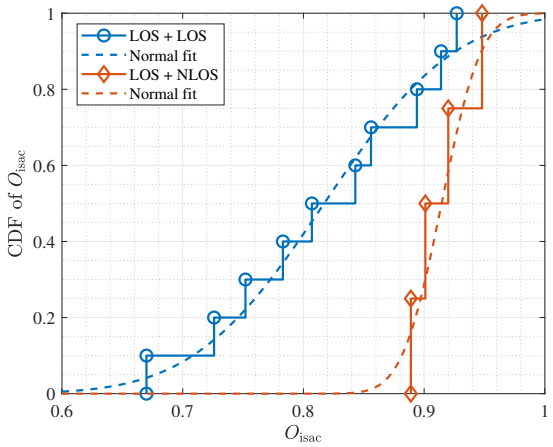

Fig. 4: CDF of the PCF. The blue and orange curves represent human target being in LOS+LOS and LOS+NLOS conditions, respectively.

Considering the realistic measurement scenario, it can be deduced that the O_{isac} value is also influenced by the following factors. Firstly, the AOD at sensing target. In a conventional communication channel, the power angle spectrum (PAS) of the Tx/Rx obeys a truncated Gaussian distribution [6]. The power of the path is higher when it is closer to the LOS path angle and lower when it is further from the LOS path angle. Hence, the smaller the angular difference between the AOD of sensing target and the LOS path angle, the bigger the power ratio of MPCs impacted by the sensing target, and the lower the O_{isac} value. For example, the O_{isac} value in position 2 (0.73) is lower than in position 9 (0.91), and in position 3 (0.67) is lower than in position 10 (0.93). Secondly, the distance between the sensing target and Tx/Rx. The research in [16] has confirmed that the farther away the sensing target is from the mono-static sensing transceiver, the easier it is to be submerged in the background environment. The same trend exists in the bi-static sensing model, e.g., the O_{isac} value is lower in position 5 (0.84) than in position 10 (0.93). Finally, the O_{isac} may also be affected by the number of sensing targets, which requires further research.

In the context of pathloss modeling for the ISAC channel, some studies suggest that it is a superposition of the pathloss from the target channel and the background channel, where the former is a concatenate pathloss model and the latter adheres to the conventional communication channel model in the 3GPP TR 38.901 [12, 13, 15, 17]. However, judging from the channel measurement observations, the background channel defined in Fig. 2 is impacted by the sensing target. If the background channel is directly reused as 3GPP TR 38.901, its pathloss would be assumed to remain constant and overestimated, which is contradictory to the observations and analysis. Hence, it is unreasonable to ignore the impact of the sensing target and apply the pathloss model in the 3GPP TR 38.901 without any modifications.

The aforementioned PCF portrays the pathloss relationship among the ISAC channel, target channel, and initial background channel. Generalizing it to the generic case, the pathloss model of ISAC channel is evolved into

$$PL_{\mathrm{isac}} = PL_{\mathrm{tar}} + PL_{\mathrm{bg}} = \sum_{i=1}^{N} PL_{\mathrm{tar}}^{i} + O_{\mathrm{isac}} \cdot PL_{\mathrm{bg}}^{38.901} \quad (3)$$

In this pathloss model, the proposed PCF characterizes the power impact of human target on the initial background channel. The PCF aims to control the power of the background channel to make the pathloss of the ISAC channel more realistic. Generally speaking, the greater the impact of the sensing target, i.e. the higher the power proportion of the target channel, the smaller the PCF within the interval of $(0, 1)$. Besides, when not introducing the sensing targets, i.e., $N = 0$, the target channel will be non-existent, and the $O_{\mathrm{isac}} = 1$. In that case, the ISAC channel is degraded to the initial background channel, which can be also treated as a conventional communication channel and modeled by the 3GPP TR 38.901. When the background channel modeling is not taken into account, e.g. there is no other EO interference from the sky in the low-altitude unmanned aerial vehicle (UAV) scenario, the ISAC channel will only contain target channel and the $O_{\mathrm{isac}} = 0$. This modeling method can decouple the target and background channels, and then allow the two parts to be recombined together by using the PCF after independent pathloss modeling, thus achieving a more reasonable pathloss modeling of the ISAC channel.

Indirect paths characteristic of target channel: For simplicity, the target-oriented PDP at each measurement position is compared with the initial background channel at the same AOD to obtain target channel. In that case, the Tx-target link can be considered as only a LOS path due to the beam focusing of the high gain horn antenna, while the propagation characteristics of the target-Rx link is the research focus.

Based on geometrical optics theory, the channel propagation paths are traced in the measurement scenario. The human target in position 3 is selected as an example, and the AOD is 80°. With a 3 dB beamwidth of 19.8°, the channel reconstruction is illustrated in Fig. 5. A total of 4 potential propagation paths are traced, which are marked with different colors. The path in red is a Tx→Rx path with a propagation distance of 10.0 m, which belongs to background channel. Except for this path, the other paths all have an interaction with human target, thus belonging to target channel. As corroborated in Fig. 5, the orange path is a Tx→human target→Rx path with a propagation distance of 10.1 m, the green path is a Tx→human target→south wall→Rx path with a propagation distance of 10.8 m and the blue path is a Tx→human target→westernmost wall→Rx path with a propagation distance of 34.3 m.

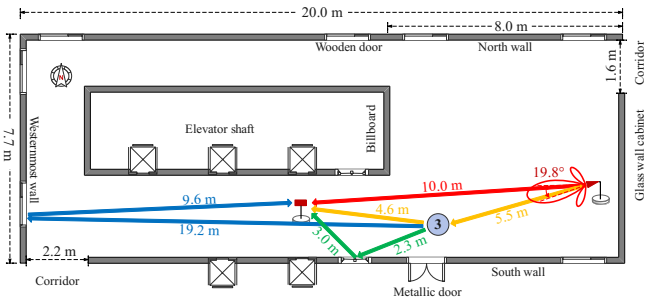

Fig. 5: Illustration of the potential propagation paths at position 3. The lines with different colours represent propagation paths of MPCs.

Corresponding to Fig. 5, Fig. 6 demonstrates the effective MPCs comparison at position 3 after denoising and peak extraction of raw PDPs. Note, that the complete processing refers to the segmented threshold denoising algorithm proposed in [18]. For simplicity and rationality, the altered paths with a cumulative PP of target channel exceeding 90% are considered. At this point, the power threshold is -118 dB, and 3 high-power paths in blue are focused on. When the human target is introduced, it's clear that one new path emerges, and the power of two original MPCs changes. Their numeral labels and absolute delays are indicated in Fig. 6. Compared to Fig. 5, these MPCs match the propagation distances and are marked with corresponding colors. Notably, path ① is a vector combination of Tx→Rx and Tx→target-Rx paths. Since its power increases compared with the original Tx→Rx path, and their distance difference is below the resolution of measurement system. Besides, the path ② and ③ are matched with the Tx→human target→south wall→Rx path and Tx→human target→westernmost wall→Rx path, respectively. The analysis confirm the existence of interactions between human target and EOs, leading to the formation of the indirect paths in target channel.

To validate the necessity of modeling indirect paths in target channel, the power proportion of each bounce MPCs in target-Rx link is counted

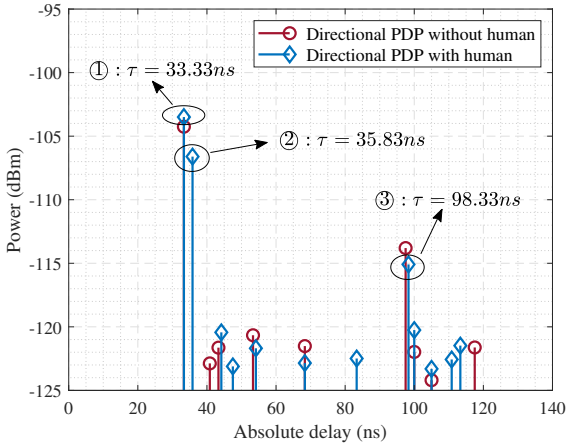

Fig. 6: Illustration of the effective MPCs comparison at position 3, where the red and blue dashed lines indicate effective MPCs in the directional PDPs without and with human target, respectively.

as

$$PP_i = \frac{P_i}{P_{\text{tar}}}, i = 0, 1, 2, \ldots, \tag{4}$$

where i is the number of scattering bounces in target-Rx link, P_i and PP_i is the power sum and power proportion of MPCs with i bounces, and P_{tar} is the total power of target channel within the target-oriented PDP. Furthermore, the position 13 is processed in the same manner with position 3, though not shown here. Then at the two positions, the power proportions of each bounces are count in Table 3.

Table 3: Power proportion of each bounce MPCs of target-Rx link

	Position 3 (LOS+LOS)	**Position 13** (LOS+NLOS)
PP_0	18.9%	0
PP_1	65.7%	16.4%
$PP_{i\geq 2}$	15.4%	83.6%

It can be observed that the power proportion of indirect paths in target channel is even over 80% at position 3, still less all MPCs are indirect paths at position 13. Their contributions to target channel cannot be underestimated. Hence, when modeling the target channel, at least in target-Rx link, it is crucial to consider the modeling of NLOS clusters.

Conclusion: In this letter, an indoor channel measurement campaign at 105 GHz is carried out to study the ISAC channel characteristics with human target impact. By comparing the PADPs with and without human target, we observe changes in the quantity and power of MPCs in the ISAC channel due to the introduction of human target. Then, we propose a factor of PCF to quantify the impact of human target on the large-scale pathloss and apply it to modify the ISAC pathloss model in existing research. The PCF combines the pathloss of target channel and background channel, making the overall pathloss of the ISAC channel more realistic. Experimental results show that the PCF follows a normal distribution within the range (0, 1) and is influenced by the condition and position of the human target. Besides, at certain points in both channel conditions, we trace back the potential propagation paths with human target in the measurement scenario and confirm them through comparative analysis of target-oriented PDPs. The power proportions of each bounce of target-Rx link within target channel support the necessity of indirect paths modeling in target channel.

Acknowledgment: This work was supported in part by the National Natural Science Foundation of China under Grants 62201087, in part by the National Natural Science Foundation of China (Grant No.92167202), in part by the National Science Foundation for Distinguished Young Scholars under Grant 61925102, in part by the National Key R&D Program of China (Grant No. 2023YFB2904803), in part by Guangdong Major Project of Basic and Applied Basic Research (No.2023B0303000001) and in part by the Beijing University of Posts and Telecommunications-China Mobile Research Institute Joint Innovation Center.

Wenjun Chen, Yuxiang Zhang, Yameng Liu, Jianhua Zhang and Huiwen Gong (*The State Key Laboratory of Networking and Switching Technology, Beijing University of Posts and Telecommunications, Beijing 100876, China*)

E-mail: jhzhang@bupt.edu.cn

Tao Jiang and Liang Xia (*China Mobile Research Institute Beijing, Beijing 100053, China*)

References

1 Liu, G., Xi, R., Han, Z., *et al.*: Cooperative Sensing for 6G Mobile Cellular Networks: Feasibility, Performance and Field Trial. *IEEE J. Sel. Areas Commun.*, Early Access (2024)
2 3GPP TSG SA: *Feasibility Study on Integrated Sensing and Communication*. 3GPP TR 22.837 (2024). Available from: https://portal.3gpp.org/desktopmodules/Specifications/SpecificationDetails.aspx?specificationId=4044
3 Serghiou, D., Khalily, M., Brown, T.W.C., Tafazolli, R.: Terahertz Channel Propagation Phenomena, Measurement Techniques and Modeling for 6G Wireless Communication Applications: A Survey, Open Challenges and Future Research Directions. *IEEE Commun. Surv. Tutorials*. **24**(4), pp. 1957-1996 (2022)
4 Zhang, J., Wang, H., Zhang, Y., *et al.*: Channel characteristics and modeling research for 6G: challenges, progress, and prospects (in Chinese). *Sci Sin Inform.*, **54**(5), pp. 1114-1143 (2024)
5 Zhang, J., Wang, J., Zhang, Y., *et al.*: Integrated Sensing and Communication Channel: Measurements, Characteristics and Modeling. *IEEE Commun. Mag.*, **62**(6), pp. 98-104 (2023)
6 Skolnik, M.I.: *Radar Handbook.*, McGraw-Hill, New York (2008)
7 Abbasi, N.A., Molisch, A.F., Zhang, J.C.: Measurement of Directionally Resolved Radar Cross Section of Human Body for 140 and 220 GHz Bands. In: 2020 IEEE Wireless Communications and Networking Conference Workshops (WCNCW), pp. 1–4. IEEE, Seoul, Korea (2020)
8 Gui, S., Yang, Y., Li, J., Zuo, F., Pi, Y.: THz Radar Security Screening Method for Walking Human Torso With Multi-Angle Synthetic Aperture. *IEEE Sens. J.*. **21**(16), pp. 17962-17972 (2021)
9 Li, X., Cui, Y., Zhang, J.A., Liu, F., Zhang D., Hanzo, L.: Integrated Human Activity Sensing and Communications. *IEEE Commun. Mag.*. **61**(5), pp. 90-96 (2023)
10 Lu, S., Liu, F., Hanzo, L.: The Degrees-of-Freedom in Monostatic ISAC Channels: NLoS Exploitation vs. Reduction. *IEEE Trans. Veh. Technol.*. **72**(2), pp. 2643-2648 (2023)
11 Lou, J., Liu, R., Jiang, C., *et al.*: A Unified Channel Model for Both Communication and Sensing in Integrated Sensing and Communication Systems. In: 2023 IEEE 98th Vehicular Technology Conference (VTC2023-Fall), pp. 1-6. IEEE, Hong Kong, Hong Kong (2023)
12 Chen, Y., Yu, Z., He, J., Yang, W., Li, J., Wang, G.: Multi-Scattering Centers Extraction and Modeling for ISAC Channel Modeling. In: 2024 18th European Conference on Antennas and Propagation (EuCAP), pp. 1-5. IEEE Glasgow, United Kingdom (2024)
13 Liu, Y., Zhang, J., Zhang, Y., Yuan, Z., Liu, G.: A Shared Cluster-Based Stochastic Channel Model for Integrated Sensing and Communication Systems. *IEEE Trans. Veh. Technol.*, **73**(5), pp. 6032-6044 (2024)
14 Hur, S., Cho, Y.-J., Lee, J., Kang, N.-G, Park, J., Benn, H.: Synchronous channel sounder using horn antenna and indoor measurements on 28 GHz. In: 2014 IEEE International Black Sea Conference on Communications and Networking (BlackSeaCom), pp. 83-87. IEEE, Odessa, Ukraine (2014)
15 3GPP RAN: *Study on channel model for frequencien from 0.5 to 100 GHz*. 3GPP TR 38.901 (2019). Available from: https://portal.3gpp.org/desktopmodules/Specifications/SpecificationDetails.aspx?specificationId=3173
16 Wang, J., Zhang, J., Zhang, Y., Jiang, T., Yu, L., Liu, G.: Empirical Analysis of Sensing Channel Characteristics and Environment Effects at 28 GHz. In: 2022 IEEE Globecom Workshops (GC Wkshps), pp. 1323–1328. IEEE, Rio de Janeiro, Brazil (2022)
17 Liu, Y., Zhang, J., Zhang, Y., Gong, H., Jiang, T., Liu, G.: How to Extend 3D GBSM to Integrated Sensing and Communication Channel with Sharing Feature?. *IEEE Commun. Lett.*, Early Access (2024)
18 Xu, H., Zhang, J., Tang, P., Tian, L., Wang, Q., Liu, G.: An Empirical Study on Channel Reciprocity in TDD and FDD Systems. *IEEE Open J. Veh. Technol.*. **5**, pp. 108-124 (2024)